ACADÉMIE
DES SCIENCES
INSTITUT DE FRANCE

Comptes Rendus
Physique

Mattheus Burkhard, Malte Kroj, Kévin Falque, Alberto Bramati, Iacopo Carusotto and Maxime J. Jacquet

Stimulated Hawking effect and quasinormal mode resonance in a polariton simulator of field theory on curved spacetime

Published online: 3 April 2026

Part of Special Issue: Simulating gravitational problems with condensed matter analog models : a special issue in memory of Renaud Parentani (1962-2020)
Guest editors: Jacqueline Bloch (Université Paris-Saclay, CNRS, Centre de Nanosciences et de Nanotechnologies, Palaiseau, France), Iacopo Carusotto (Pitaevskii BEC Center, INO-CNR, Trento, Italy) and Chris Westbrook (Laboratoire Charles Fabry de l'Institut d'Optique, Palaiseau, France)

https://doi.org/10.5802/crphys.278

CENTRE MERSENNE
The Comptes Rendus. Physique *are a member of the Mersenne Center for open scientific publishing*
www.centre-mersenne.org — e-ISSN : 1878-1535

ACADÉMIE DES SCIENCES
INSTITUT DE FRANCE

Comptes Rendus. Physique
Published online: 3 April 2026
https://doi.org/10.5802/crphys.278

Research article / *Article de recherche*

Simulating gravitational problems with condensed matter analog models : a special issue in memory of Renaud Parentani (1962-2020) / *Simuler des problèmes gravitationnels avec des modèles analogues en matière condensée : un numéro spécial en mémoire de Renaud Parentani (1962-2020)*

Stimulated Hawking effect and quasinormal mode resonance in a polariton simulator of field theory on curved spacetime

Effet Hawking stimulé et résonance d'un mode quasinormal dans un simulateur polaritonique de théorie des champs en espace courbe

Mattheus Burkhard [#,a,b], Malte Kroj [#,c], Kévin Falque [c], Alberto Bramati [c], Iacopo Carusotto [a] and Maxime J. Jacquet [*,c]

[a] Pitaevskii BEC Center, CNR-INO and Dipartimento di Fisica, Università di Trento, 38123 Trento, Italy

[b] Université Paris Cité, CNRS, Matériaux et Phénomènes Quantiques, 75013 Paris, France

[c] Laboratoire Kastler Brossel, Sorbonne Université, CNRS, ENS-Université PSL, Collège de France, Paris 75005, France

E-mail: maximjacquet@gmail.com

Abstract. The Hawking effect amplifies fluctuations in the vicinity of horizons, both in black holes and in analogue platforms. Here, we consider a polariton simulator and numerically examine the *stimulated* Hawking effect using a coherent probe incident on the horizon from the exterior. We implement an experimentally realistic effective spacetime that supports a quasinormal mode (QNM) in the vicinity of the horizon. We find that the stimulated Hawking effect manifests as transmission into a negative-energy Bogoliubov channel inside the horizon, consistent with pseudo-unitary Bogoliubov scattering. Moreover, transmission across the horizon peaks at the QNM frequency. The computed spectral signatures provide a practical guide for future experimental investigations of the Hawking effect and its interplay with QNMs, an open question in quantum field theory in curved spacetime.

Résumé. L'effet Hawking amplifie les fluctuations au voisinage des horizons, aussi bien dans les trous noirs astrophysiques que dans leurs plateformes analogues. Nous considérons ici un simulateur polaritonique et examinons numériquement l'effet de Hawking *stimulé* par une sonde cohérente incidente sur l'horizon

[#] Contributed equally

[*] Corresponding author

depuis l'extérieur. Nous considérons un espace-temps effectif expérimentalement réaliste qui supporte un mode quasinormal (QNM) au voisinage de l'horizon. Nous montrons que l'effet Hawking stimulé se manifeste par une transmission vers un canal de Bogolioubov d'énergie négative à l'intérieur de l'horizon, conformément à une diffusion de Bogolioubov pseudo-unitaire. De plus, la transmission à travers l'horizon présente un maximum à la fréquence du QNM. Les signatures spectrales calculées fournissent un guide pratique pour de futures investigations expérimentales de l'effet Hawking et de son interaction avec les QNMs, question encore ouverte dans le cadre de la théorie quantique des champs en espace-temps courbe.

Keywords. Hawking radiation, analogue gravity, quantum fluids of light, quasinormal modes, numerical simulations.

Mots-clés. Effet Hawking, gravité analogue, théorie quantique des champs, polaritons en microcavité semi-conductrice, simulation numérique, modes quasinormaux.

Funding. Provincia Autonoma di Trento & National Quantum Science and Technology Institute (PNRR MUR Project, Grant Number: PE0000023-NQSTI); EU Pathfinder (Grant Number: 101115575 Q-One).

Manuscript received 15 November 2025, revised 26 February 2026, accepted 10 March 2026.

Introduction

In recent years, analogue-gravity systems have provided a compelling platform for studying quantum-field dynamics in curved spacetimes [1–3]. Such experiments have brought within laboratory reach phenomena traditionally confined to astrophysical scales, most notably the Hawking effect [4–9]. Although early theoretical work focused on the scattering of vacuum fluctuations in both conservative and driven-dissipative quantum fluids [10–30], experiments have also probed these systems with externally injected fields to *stimulate* the Hawking process and to obtain frequency-resolved insights into the underlying physics [4–7,31].

In this work, we study the stimulated Hawking process at a horizon in a polaritonic quantum fluid of light by injecting a weak monochromatic field. We numerically model a pump-probe configuration in which a downstream support field maintains an approximately constant density, a regime previously identified as favourable for spontaneous emission. In contrast to earlier work dominated by vacuum radiation, the probe provides a frequency-resolved read-out of scattering in the asymptotic modes. We find a crossover from two-port *unitary* scattering (no negative-norm channel available) at $\omega > \omega_{\max}$ to *pseudo-unitary* scattering with negative-norm participation at $\omega < \omega_{\max}$, with $\omega_{\max}$ determined by the transcritical flow [32]. Here, $\omega_{\max}$ denotes the upper frequency bound for which mixed-norm scattering channels exist asymptotically; above $\omega_{\max}$ only positive-norm channels remain, and Hawking-type amplification is unavailable. Moreover, transmission into the supercritical region exhibits a pronounced resonance at the quasinormal-mode frequency $\omega_{\mathrm{qnm}} > \omega_{\max}$, i.e. outside the Hawking-emission window [33]. This enables a direct comparison between horizon and horizonless emission — expected to display distinct correlation structures [34] — and recasts the QNM as an active mediator of stimulated scattering rather than a passive geometric fingerprint.

1. The polaritonic simulator

Exciton-polaritons (polaritons) arise in planar semiconductor microcavities from the strong coupling between quantum-well excitons and cavity photons. Their hybrid light-matter character yields a small effective mass and sizeable nonlinearity, enabling collective phenomena akin to

those in atomic Bose–Einstein condensates, but within optical platforms. Under coherent driving and dissipation, the dynamics of the polariton field $\psi(x,t)$ is governed by a driven-dissipative Gross–Pitaevskii equation (GPE) [35]

$$i\hbar\partial_t\psi = \left[\hbar\omega_0 - \frac{\hbar^2}{2m^*}\partial_x^2 + V(x) + \hbar g\,|\psi|^2 - \frac{i\hbar\gamma}{2}\right]\psi + \hbar F(x)\,e^{-i\omega_{\rm p}t}, \tag{1}$$

with effective mass m^*, interaction constant $g > 0$ (defined so that the interaction-induced blueshift is $\hbar g|\psi|^2$), loss rate γ, lower-polariton frequency ω_0 at zero in-plane wave-vector, and a structured pump envelope $F(x)$ of frequency $\omega_{\rm p}$. We approximate the lower-polariton dispersion as $\omega_{\rm LP}(k) \simeq \omega_0 + \hbar k^2/(2m^*)$.

For a plane-wave pump $F(x) = F_{\rm p}e^{ik_{\rm p}x}$ of constant amplitude $F_{\rm p}$ (stationary in the rotating frame), the steady flow $\psi_0 = \sqrt{n_0}\,e^{i(k_{\rm p}x-\omega_{\rm p}t)}$ yields the equation of state

$$n_0\left[\left(gn_0 - \delta(v_0)\right)^2 + \frac{\gamma^2}{4}\right] = |F_{\rm p}|^2. \tag{2}$$

Here $\delta(v_0) = \omega_{\rm p} - \omega_0 - \frac{m^* v_0^2}{2\hbar}$ is the effective detuning, and the hydrodynamic velocity is $v_0 = \hbar\partial_x\phi/m^* = \hbar k_{\rm p}/m^*$, where $\phi(x)$ is the phase of the stationary field ψ_0 (for a plane wave, $\phi = k_{\rm p}x$). When $\delta/\gamma > \sqrt{3}/2$, the input-output curve is bistable (S-shaped) with a stable upper branch (see Figure 1(a)), used below as the high-density state.

We study collective excitations by linearising around a stationary background with the ansatz

$$\psi(x,t) = e^{i(k_{\rm p}x-\omega_{\rm p}t)}\left[\sqrt{n_0(x)} + \delta\psi(x,t)\,e^{-\gamma t/2}\right], \qquad \delta\psi = u(x)\,e^{-i\omega t} + v^*(x)\,e^{+i\omega t}. \tag{3}$$

In a spatially inhomogeneous system (spatially varying $v_0(x)$ and $c_{\rm B}(x)$), the Bogoliubov spinor $\binom{u}{v}$ obeys [32]

$$\mathscr{L}\begin{pmatrix}u\\v\end{pmatrix} = \hbar\omega\begin{pmatrix}u\\v\end{pmatrix}, \qquad \mathscr{L} = \begin{pmatrix}-\hbar\delta(v_0) + 2\hbar g n_0 + D & \hbar g n_0\\ -\hbar g n_0 & -\left[-\hbar\delta(v_0) + 2\hbar g n_0 + D\right]^*\end{pmatrix}, \tag{4}$$

with the differential operator $D = -\frac{\hbar^2}{2m^*}\partial_x^2 - i\hbar\,v_0(x)\,\partial_x - i\frac{\hbar}{2}\,\partial_x v_0(x)$, where the last term is local and purely imaginary; it vanishes in homogeneous regions and is appreciable only where $v_0(x)$ varies significantly (e.g. near the horizon) [36]. In what follows, we employ a local-density approximation (LDA) to obtain analytic laboratory-frame dispersions; within the LDA we neglect $\partial_x v_0$ and treat n_0, v_0 as piecewise constant when deriving the dispersion relation.

We identify a *Killing horizon* at the position where $|v_0| = c_{\rm B}$. In a slowly varying inhomogeneous flow, applying the LDA to (4) yields the laboratory-frame dispersion relation

$$\omega_\pm^{\rm B}(k;x) = v_0(x)\,k \pm \sqrt{\left[\frac{\hbar k^2}{2m^*}\right]^2 + c_{\rm B}^2(x)\,k^2 + c_{\rm B}^2(x)\,\frac{m_{\rm det}^2(x)}{\hbar^2}}, \tag{5}$$

where the Bogoliubov light-cone velocity $c_{\rm B}$ sets the causal bound $|\partial\omega/\partial k| \le c_{\rm B}(x)$ and the mass parameter $m_{\rm det}$ encodes the local mass gap [32]:

$$c_{\rm B}(x) = \sqrt{\frac{\hbar\left[2gn_0(x) - \delta\big(v_0(x)\big)\right]}{m^*}}, \qquad m_{\rm det}(x) = m^*\,\frac{\sqrt{[gn_0-\delta][3gn_0-\delta]}}{2gn_0-\delta}\bigg|_x. \tag{6}$$

The effective geometry is captured by the Painlevé–Gullstrand line element [37]

$$\mathrm{d}s^2 = \left[c_{\rm B}^2(x) - v_0^2(x)\right]\mathrm{d}t^2 - 2\,v_0(x)\,\mathrm{d}x\,\mathrm{d}t - \mathrm{d}x^2. \tag{7}$$

As in all analogue simulators, the presence of a horizon is signalled by the excitation of negative-norm modes $\omega_-^{\rm B}$ at positive frequencies, i.e. negative-energy waves [32].

Notation. We denote the outside positive-norm channel by u_+ and the inside channels by d_+ (positive) and d_- (negative).

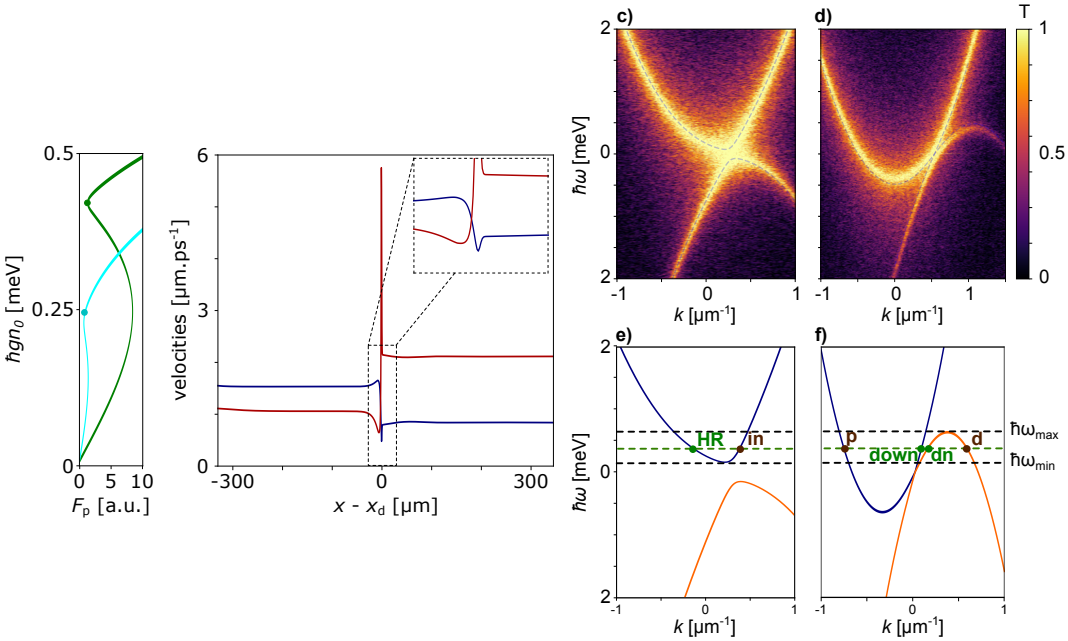

Figure 1. Polariton mean-field. Mean-field profile with downstream density support. (a) Bistability loop for $k_{\mathrm{up}} = 0.27\,\mu\mathrm{m}^{-1}$ (green) and $k_{\mathrm{down}} = 0.539\,\mu\mathrm{m}^{-1}$ (turquoise). (b) Bogoliubov sound speed c_{B} (blue) and background fluid velocity v_0 (red). **Dispersion of Bogoliubov excitations**. (c)–(d) The colour map shows the normalised spectral density $T(k,\omega)$ of the fluctuation field, revealing the numerical dispersion relation; dashed lines show the LDA prediction (5); (c) upstream; (d) downstream. (e)–(f) LDA dispersion. Blue: positive-norm modes ω_+^{B}; orange: negative-norm modes ω_-^{B}. Brown dots: *in* modes **in** (upstream), **p** and **d** (downstream); green dots: *out* modes **HR** (upstream), **down** and **dn** (downstream). We stimulate the Hawking effect by injecting a finite-amplitude continuous-wave (CW) probe into the input mode **in**.

2. Numerical simulation of the mean-field and Bogoliubov spectrum

We now simulate polariton dynamics in a one-dimensional (1D) sample (e.g. a wire or effective 1D propagation). We use *Julia* to integrate the (1+1)D GPE with a split-step scheme on a 2048-point grid (cavity length 800 μm), with absorbing boundary conditions. As in [28,33], we take $m^* = 5\times10^{-35}$kg, $\hbar\omega_0 = 1473.36$ meV, $\hbar\gamma = 47\,\mu$eV and $\hbar g = 3\times10^{-4}$ meV μm. $V(x)$ is an attractive Gaussian potential (height -0.85 meV, width 0.75 μm) centred at $x_{\mathrm{d}} = 400\,\mu$m. We refer to it as "the defect".

We employ a structured pump: high constant intensity for $x < x_{\mathrm{d}} - 7\,\mu$m and low constant intensity for $x > x_{\mathrm{d}} - 7\,\mu$m. The pump frequency is $\hbar\omega_{\mathrm{p}} = 1473.85$ meV, while its wave-vector is structured as $k_{\mathrm{up}} = k_{\mathrm{p}}(x < x_{\mathrm{d}} - 7\,\mu\mathrm{m}) = 0.27\,\mu\mathrm{m}^{-1}$ and $k_{\mathrm{down}} = k_{\mathrm{p}}(x > x_{\mathrm{d}} - 7\,\mu\mathrm{m}) = 0.539\,\mu\mathrm{m}^{-1}$ (this specific value of k_{down} was chosen to match the phase across the horizon and to produce an approximately flat downstream density; see the appendix of [28] for details).

Figure 1(a) shows optical bistability for effective detunings $\hbar\delta(v_{\mathrm{up}}) = 0.39$ meV (green) and $\hbar\delta(v_{\mathrm{down}}) = 0.12$ meV (cyan). Upstream, the pump intensity $F_{\mathrm{p,up}}$ is set 0.08% above the turning point (green dot) to stabilise a steady state. Downstream, in the supported case, $F_{\mathrm{p}}(x > x_{\mathrm{d}} - 7\,\mu\mathrm{m})$ is 16% above the turning point (cyan dot). *These percentages are not directly comparable:* 0.08% is an input-intensity offset on the upstream S-curve, whereas 16% corresponds to an effective-

detuning offset in the downstream supported region; because the S-curve slopes differ by $\mathcal{O}(10^2)$ across the horizon, a small upstream fractional shift maps to a much larger downstream relative offset.

Figure 1(b) shows v_0 (red) and c_B (blue). As the fluid flows from left to right with increasing velocity, by analogy with a waterfall we refer to the high-density region as upstream and the low-density region as downstream. Downstream, $v_{\rm down}$ reaches a constant value of $2.07\,\mu\mathrm{m\,ps}^{-1}$ set by $k_{\rm down}$ and exceeds c_B, which is supported at a constant value of $0.81\,\mu\mathrm{m\,ps}^{-1}$. The attractive defect causes a dip in the sound speed (equivalently, in the density) at x_d, accompanied by a spike in the fluid velocity under quasi-conservation of the current (see the inset in Figure 1(b)). Section 4 discusses the impact of these narrow features on the emission spectrum.

We probe the Bogoliubov dispersion by adding a weak complex Gaussian white-noise term (uncorrelated in space and time) at each time step of the GPE evolution, which excites linear fluctuations without altering the mean-field profile. After discarding transients, we compute the spatiotemporal Fourier transform of the fluctuation field $\delta\psi(x,t) = \psi(x,t) - \psi_0(x,t)$ in a given asymptotic region $r \in \{\mathrm{up}, \mathrm{down}\}$ using a Hann spatial window $w_r(x)$: $A_r(k,\omega) = \int \mathrm{d}t \int \mathrm{d}x\, w_r(x)\, \delta\psi(x,t)\, e^{i(\omega t - kx)}$. The colour maps in Figure 1(c)–(d) show the normalised spectral density $T_r(k,\omega) = |A_r(k,\omega)|^2 / \max_{k,\omega}|A_r(k,\omega)|^2$ (so $0 \le T_r \le 1$). We restrict the spatial Fourier transform to obtain *local* spectra in the upstream (Figure 1(c)) and downstream (Figure 1(d)) regions. As the integration time is arbitrary, we normalise the spectral intensity to its maximum, enabling qualitative comparison only. Upstream (Figure 1(c)), the spectrum is slightly gapped, as expected for a pump intensity near but not at the bistability turning point. A comparable gap is visible downstream when the fluid density is supported by a finite pump (Figure 1(d)).

Assuming piecewise-homogeneous density and flow in each spatial region, the LDA gives the real part of the spectrum (5). We see in Figure 1(c) that the LDA captures the spectrum well when the density is high. When the density is low (Figure 1(d)), the LDA slightly overestimates the Mach number, yet the agreement with numerical data remains good (in line with spectral measurements in inhomogeneous media in [32,36]). In what follows, we base our discussion on the LDA spectrum in Figure 1(e)–(f).

Because of the Doppler effect, the downstream transcritical flow shifts $\omega_-^{\rm B}$ solutions (orange) to positive frequencies up to $\omega_{\rm max}$. Within $\omega_{\rm min} < \omega < \omega_{\rm max}$ (bounded below by the upstream gap $\omega_{\rm min}$), there are three *input* modes (brown): **in** ($\omega_+^{\rm B}$) propagating towards the horizon upstream, and **p** ($\omega_+^{\rm B}$) and **d** ($\omega_-^{\rm B}$) propagating against the supercritical flow downstream. There are also three *output* modes (green): **HR** ($\omega_+^{\rm B}$) propagating away from the horizon upstream, and **down** ($\omega_+^{\rm B}$) and **dn** ($\omega_-^{\rm B}$) propagating inside the horizon downstream. Thus, over $\omega_{\rm min} < \omega < \omega_{\rm max}$, positive- and negative-norm modes coexist at positive frequencies. This signals the formation of a Killing horizon for the Bogoliubov modes [32].

3. The stimulated Hawking effect

The Hawking effect arises from the scattering of incoming waves at the horizon, which mixes $\omega_+^{\rm B}$ and $\omega_-^{\rm B}$ solutions of Eq. (5) via the scattering matrix S. A key feature is its pseudo-unitarity, dictated by conservation of the Bogoliubov scalar product,

$$\langle \phi_1 | \phi_2 \rangle = \int \mathrm{d}x\, (u_1^* u_2 - v_1^* v_2), \tag{8}$$

which is indefinite and classifies modes into positive- and negative-norm branches, $\omega_+^{\rm B}$ and $\omega_-^{\rm B}$, respectively [38]. We now outline how dispersion controls scattering at the horizon and, in turn, how Hawking-type amplification arises.

The dispersion in Figure 1(e)–(f) implies that the properties of S depend on frequency:

- $\omega < \omega_{\min}$: only downstream channels propagate; **p** and **d** are incoming, while **down** and **dn** are outgoing; Eq. (8) leads to anomalous mixing described by a 2×2 matrix obeying $S^\dagger \operatorname{diag}(1,-1) S = \operatorname{diag}(1,-1)$;
- $\omega_{\min} < \omega < \omega_{\max}$: there are three input modes (**in**, **p**, **d**) and three output modes (**HR**, **down**, **dn**). **HR** is the unique upstream outgoing channel (Hawking radiation); pseudo-unitarity reads $S^\dagger \operatorname{diag}(1,1,-1) S = \operatorname{diag}(1,1,-1)$;
- $\omega > \omega_{\max}$: only positive-norm channels remain, and scattering reduces to a two-port unitary process.

For $\omega < \omega_{\max}$, pseudo-unitarity entails mixing of creation and annihilation operators. For example, when $\omega_{\min} < \omega < \omega_{\max}$,

$$\begin{pmatrix} \widehat{a}_{\mathbf{HR}} \\ \widehat{a}_{\mathbf{down}} \\ \widehat{a}^\dagger_{\mathbf{dn}} \end{pmatrix} = S \begin{pmatrix} \widehat{a}_{\mathbf{in}} \\ \widehat{b}_{\mathrm{vac},\mathbf{p}} \\ \widehat{b}^\dagger_{\mathrm{vac},\mathbf{d}} \end{pmatrix}. \tag{9}$$

In the language of Gaussian quantum optics, this mixing is a concatenation of two symplectic operations: (i) a two-mode squeezer, responsible for pair creation across the horizon; (ii) a beam splitter, describing partial transmission through the effective potential barrier.

The probe cannot be injected from upstream for $\omega < \omega_{\min}$. For $\omega > \omega_{\min}$, a coherent monochromatic probe $|\eta_{\mathbf{in}}\rangle$ can be injected from upstream. Considering that all other positive- and negative-norm input modes are in the vacuum state, the input state is $|\rho_{\mathrm{in}}\rangle = |\eta_{\mathbf{in}}\rangle \otimes |0_{\mathbf{p}}\rangle \otimes |0_{\mathbf{d}}\rangle$. For $\omega_{\min} < \omega < \omega_{\max}$, Eq. (9) shows that the incoming excitation is scattered into the reflected upstream mode (**HR**) and into two transmitted downstream modes (**down**, **dn**). Crucially, conservation of the Bogoliubov scalar product implies that population of **dn** is necessarily accompanied by a net increase of the energy flux in co-propagating positive-norm channels, i.e. amplification. For $\omega > \omega_{\max}$, unitarity of the 2×2 S-matrix forbids amplification, and the interface acts as a simple beam splitter.

Although the simulations use classical waves, the gain originates from mixing between positive- and negative-norm channels — the classical counterpart of parametric (squeezing) processes. In particular, the gain is frequency-dependent and, in our configuration, peaks near the near-horizon resonance frequency Ω_{qnm} (see Figure 2(e)). However, like other superradiant processes [39], although ω is conserved, k is not.

4. Quasinormal modes and resonant transmission

Quasinormal modes (QNM) are the natural resonances of open-wave systems: they solve linearised equations with purely outgoing boundary conditions and have complex frequencies $\widetilde{\omega}_{\mathrm{qnm}} = \Omega_{\mathrm{qnm}} - i\,\Gamma_{\mathrm{qnm}}/2$ [40,41]. They enter our problem as poles of the horizon scattering matrix and control the long-lived response of the driven-dissipative polariton fluid.

In the present configuration, the attractive defect generates a narrow density dip and a companion spike in the flow velocity just inside the horizon (Figure 1(b), inset). This forms a short, leaky resonator bounded by higher-density "shoulders": impedance mismatches on either side partially reflect Bogoliubov waves while allowing leakage into the upstream and downstream asymptotic regions. The QNMs are the resonant standing-wave solutions located in this region and radiating outward [33]: here, the QNMs are zero-norm modes composed of a localized negative-norm mode coupled to propagating positive-norm modes on either side of the horizon. Semiclassically, they satisfy a lossy round-trip condition, which fixes a complex eigenfrequency; equivalently, they appear as simple poles of the relevant scattering amplitudes. In practice, Ω_{qnm} lies slightly above the upper edge $\omega_{\max}$ of the Hawking window. This is not accidental:

the strong velocity spike inside the horizon Doppler-shifts the negative-norm branch to positive laboratory frequencies above $\omega_{\max}$, enabling a localised negative-norm component even though the asymptotic **dn** channel is closed for $\omega > \omega_{\max}$. The linewidth $\Gamma_{\rm qnm}$ contains contributions from both intrinsic polariton losses and radiative leakage through the shoulders; for the present parameters they are comparable, so $\Gamma_{\rm qnm}$ is of order γ [33].

Consider a weak monochromatic probe injected in the upstream input mode **in**. For $\omega > \omega_{\max}$ the interface reduces to a two-port unitary scatterer between the incoming set $\{\mathbf{in}, \mathbf{p}\}$ and the outgoing set $\{\mathbf{HR}, \mathbf{down}\}$ (no negative-norm channel is available), so there is no net amplification, only redistribution between reflection and transmission. In the single-sided drive used here, only **in** is populated; the internal incidence channel **p** is left in vacuum. In this regime, the complex transmission coefficient in **down** acquires a Breit–Wigner contribution [41], $t_{\rm in\to down}(\omega) \simeq t_{\rm bg}(\omega) + \frac{\alpha}{\omega - \Omega_{\rm qnm} + i\Gamma_{\rm qnm}/2}$, with a π-phase slip across $\Omega_{\rm qnm}$ and a peak height/width governed by $Q = \Omega_{\rm qnm}/\Gamma_{\rm qnm}$. The corresponding intensity exhibits a narrow maximum at $\omega = \Omega_{\rm qnm}$, i.e. a frequency-resolved spectroscopy line outside the spontaneous-emission band. This mechanism differs from ordinary tunnelling: it is mediated by a long-lived intermediate state set by the near-horizon geometry.

In momentum-resolved measurements, this appears as a sharp, frequency-selected enhancement along the upstream and downstream $\omega^{\rm B}_{+}$ loci, without concomitant growth of **dn** at the same ω (the latter being kinematically closed).[1] This separation in (k, ω) mirrors the outgoing-channel mapping discussed earlier and provides a practical diagnostic for experiments.

The QNM therefore plays a dual role: sets a privileged frequency just above $\omega_{\max}$ at which probe transmission and reflection are resonantly enhanced and rotate in phase, and provides a geometric handle on the near-horizon structure (through $\Omega_{\rm qnm}$ and $\Gamma_{\rm qnm}$). We now extract $\widetilde{\omega}_{\rm qnm}$ from the linear problem and verify the predicted peak and phase behaviour of $t_{\rm in\to down}(\omega)$ numerically.

5. Numerical simulation of scattering at the horizon

We now discuss the scattering of a low-amplitude continuous-wave (CW) probe sent towards the horizon from upstream, i.e. in mode **in**. The probe amplitude is set to $|F_{\rm pr}| = 0.1\% |F_{\rm p,up}|$ so as to minimally perturb the mean field. The probe is a 12 µm Gaussian centred on $x_{\rm pr} = x_{\rm d} - 100\,\mu$m. Bogoliubov excitations created by the probe propagate toward the horizon with group velocity $v_g(k_{\rm pr}) = \frac{\partial\omega}{\partial k}$.

The simulation proceeds as follows: we first integrate the GPE with the source term $F_{\rm p,up}$ only, until a steady state is reached. For each $k_{\rm pr}, \omega_{\rm pr}$, we then add a second source term $F_{\rm pr}$ with $\omega_{\rm pr} = \omega(k_{\rm pr})$, and allow the system to relax to a new steady state. We then continue the time evolution and perform space-time Fourier transforms of $\psi - \psi_0$ to obtain amplitudes $A(k, \omega)$ in the up- and downstream regions, retrieved by windowed spatial Fourier analysis (Hann window).

This procedure effectively simulates the scattering of **in** amplitude into the outgoing modes **HR**, **dn** and **down**, as in an experiment. This procedure provides the experimentally accessible spectral weight of the physical field $\delta\psi$, but it does not directly yield the flux-normalised Bogoliubov scattering amplitudes: extracting the S-matrix would require projecting onto incoming/outgoing BdG eigenvectors and normalising by the conserved current.

[1] For completeness, we summarise the frequency-dependent availability of asymptotic channels and the role of the local Doppler shift of the $\omega^{\rm B}_{-}$ branch near the horizon. For $\omega < \omega_{\min}$ only downstream channels propagate; for $\omega_{\min} < \omega < \omega_{\max}$, mixed-norm scattering is possible with one upstream outgoing channel (HR) and two downstream outgoing channels (down, dn); for $\omega > \omega_{\max}$ only positive-norm channels persist asymptotically. Locally, the Doppler spike can bring parts of $\omega^{\rm B}_{-}$ to positive laboratory frequency, enabling norm-mixing inside the near-horizon resonator; asymptotically, however, **dn** closes above $\omega_{\max}$, and scattering reduces to a two-port unitary process.

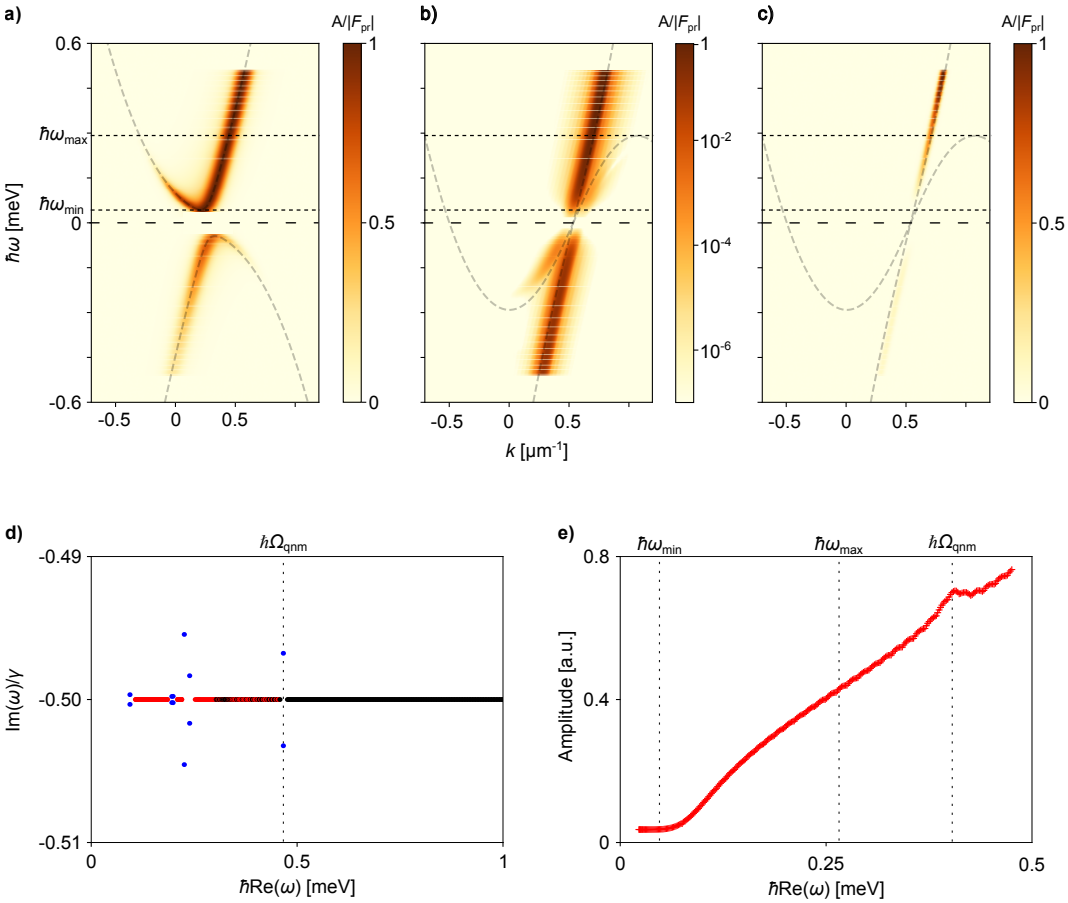

Figure 2. Numerical simulation of scattering. Amplitude is injected in mode **in** at $k_{\rm pr}$, $\omega_{\rm pr}$ and allowed to scatter at the horizon. Amplitudes are normalised to the probe amplitude. All $\omega_{\rm pr}$ slices are collated to form the spectra in each region. (a) Amplitude upstream (linear scale). (b) Amplitude downstream (log scale). (c) Amplitude downstream (linear scale). Dashed lines: LDA dispersion (5). **Spectral properties of the quasinormal mode**. (d) Spectrum of Bogoliubov excitations. Red: negative-norm; black: positive-norm; blue: zero-norm. Zero-norm modes at low frequency are spurious artefacts of the numerical boundaries and are localised outside the near-horizon region. The response near $\omega_{\rm qnm}$ is a *damped QNM* response of the Bogoliubov field. (e) Amplitude in mode **down**.

Figure 2 shows the simulation results. The amplitude is normalised to the input amplitude. Gaps in the spectra reflect cases where the resonance search fails at a given $k_{\rm pr}, \omega_{\rm pr}$, in which case the run is omitted. Dashed lines show the LDA dispersion. Reflected amplitudes broadly follow the LDA prediction. In the downstream window, two branches can lie close in (k,ω); because the windowed spatial Fourier transform has finite k-resolution (spectral leakage), their contributions overlap and add coherently at the level of the complex amplitude, $A(k,\omega) \sim A_1\, W(k-k_1) + A_2\, W(k-k_2)$, where W is the Fourier transform of the spatial window. The resulting cross term in $|A|^2$ produces an asymmetric (Fano-like) modulation and can slightly bias the apparent peak position along k. A similar effect may occur in experimental data; however, the integrated transmission spectrum versus ω is unaffected and remains a robust observable of the underlying physics.

Consider the top row of Figure 2: (a) shows the upstream amplitude (linear scale), while (b) (resp. (c)) shows the downstream amplitude on logarithmic (resp. linear) scale. In (a), the probe is injected from $\omega_{\min}$ (below which injection is not possible). Comparing (a) and (c), the amplitude is predominantly reflected into **HR** up to $\hbar\omega \approx 0.25\,\text{meV}$; at higher frequencies, it is chiefly transmitted into **down**. In (b), a finite amplitude is also transmitted into **dn**, the hallmark of Hawking-type amplification.

In Figure 2(b), non-negligible amplitude appears in **down*** and **dn*** (at negative ω), as expected in Bogoliubov theory. Because **dn** is a negative-norm mode with $|v| > |u|$, the field weight resides mainly in the conjugate component; consequently the **dn*** trace is generically stronger than **dn** itself, a trend enhanced when downstream support separates the $\omega_\pm$ branches.

For $\omega > \omega_{\max}$, reflection drops to zero and the probe amplitude is transmitted downstream into **down**. As discussed in Section 3, at these frequencies the interface between sub- and supercritical flows is no longer a horizon (no negative-norm mode is available at positive frequencies) and acts as a simple beam splitter. Scattering is then dominated by transmission in **down**, with a very small reflected amplitude (of order 10^{-3} here), and no amplification occurs.

6. Numerical observation of resonant scattering

Section 3 established that for $\omega > \omega_{\max}$ scattering at the interface is unitary, and Section 5 showed that the input amplitude is then transmitted downstream into **down**. Section 4 further anticipates a QNM signature: an enhancement of transmission into **down**.

The spectral properties of the QNM are shown in Figure 2. In (d), we diagonalise the Bogoliubov matrix and obtain its eigenmodes. Positive-norm modes are shown in black, negative-norm modes in red, and zero-norm modes in blue. Zero-norm modes at low frequency ($< 0.2\,\text{meV}$) are artefacts of the periodic boundary conditions in the diagonalisation. The QNM is the only zero-norm mode at higher frequencies, just above $\omega_{\max}$. Here, $\Gamma_{\text{qnm}}/2$ is only slightly different from the intrinsic polariton losses. Thus, linear losses set the QNM linewidth (Γ_{qnm}) and prevent dynamical runaway inside the near-horizon resonator. In (b), we show the amplitude in **down**, retrieved from Figure 2(e). The amplitude is zero before $\omega_{\min}$ and then increases monotonically with ω, with a peak at Ω_{qnm}. This confirms resonant transmission.

Repeating the calculations without downstream density support yields the same qualitative and quantitative features. Beyond the QNM line itself, all other observables (mode splitting, channel mapping, frequency windows) are likewise robust to the presence or absence of support. This robustness indicates that the QNM is not an artefact of boundary pumping, but a structural feature of the effective spacetime geometry.

In summary, the spectral peak at $\omega = \Omega_{\text{qnm}}$ confirms that the QNM arises from the internal geometry of the polariton fluid rather than from extrinsic gain.

7. Conclusions

We have theoretically validated the feasibility of observing stimulated Hawking radiation in a realistic polariton platform using frequency-resolved probe spectroscopy. Horizon scattering in our driven polariton fluid shows high reflectivity into **HR** at low frequencies, accompanied by transmission into **dn** (the negative-norm partner), while the downstream amplitude is dominated by the positive-norm witness mode **down** [22,42]. With downstream density support, the separation of $\omega^\pm$ branches by the mass gap, and the concomitant increase in interaction energy, enhance the visibility of **dn**. This support is experimentally feasible, strengthening the case for polariton platforms as analogue quantum-field simulators on tailored curved spacetimes and enabling systematic studies of how horizon configurations imprint the Hawking spectrum [33,42–48].

In the present transcritical geometry, a narrow near-horizon resonator supports a quasinormal mode of the Bogoliubov field [33]. Our simulations show a pronounced frequency-resolved peak in the stimulated transmission in **down** at $\omega = \Omega_{\mathrm{qnm}}$, outside the Hawking-emission interval. This enables diagnosis of the effective geometry by transmission spectroscopy, an analogue of black-hole spectroscopy. The QNM thus plays a dual role: it is both a dynamical signature of the Killing horizon and an active mediator of amplification. Its frequency sets a privileged scale at which the near-horizon geometry becomes dynamically relevant, providing a resonant fingerprint of the engineered curved spacetime. As the required conditions have already been demonstrated [32], these effects should be accessible to current experiments, offering a platform for addressing open questions in near-horizon physics [33,49–51].

Acknowledgments

We thank Quentin Valnais, Malo Joly, and Tangui Aladjidi for assistance with the numerical code, and Marcos Gil de Olivera, Killian Guerrero, and Elisabeth Giacobino for insightful discussions on the dynamics of quantum fluids of light. Our investigations were inspired in large part by Renaud Parentani's work on quantum fluids in analogue gravity; the references cited here reflect only a subset of his and his collaborators' contributions to the field.

A.B. is a fellow of the Institut Universitaire de France. I.C. is supported by the Provincia Autonoma di Trento and by the Q@TN initiative and acknowledges financial support from Provincia Autonoma di Trento (PAT) and from the National Quantum Science and Technology Institute through the PNRR MUR project under Grant PE0000023-NQSTI, co-funded by the European Union – NextGeneration EU. M.J.J. and A.B. are supported by Ile de France DIM SIRTEQ, and acknowledge funding from EU Pathfinder 101115575 Q-One, the DIM SIRTEQ project FOLIAGE, and CNRS via an 80^{prime} PhD studentship. A.B. also acknowledges support from the Institut Universitaire de France.

Declaration of interests

The authors do not work for, advise, own shares in, or receive funds from any organization that could benefit from this article, and have declared no affiliations other than their research organizations.

References

[1] C. Barceló, S. Liberati and M. Visser, "Analogue Gravity", *Living Rev. Relativ.* **14** (2011), article no. 3 (159 pages).

[2] M. J. Jacquet, S. Weinfurtner and F. König, "The next generation of analogue gravity experiments", *Philos. Trans. R. Soc. Lond., Ser. A* **378** (2020), no. 2177, article no. 20190239 (7 pages).

[3] C. R. Almeida and M. J. Jacquet, "Analogue gravity and the Hawking effect: historical perspective and literature review", *Eur. Phys. J. H* **48** (2023), article no. 15.

[4] T. G. Philbin, C. Kuklewicz, S. Robertson, S. Hill, F. König and U. Leonhardt, "Fiber-Optical Analog of the Event Horizon", *Science* **319** (2008), pp. 1367–1370.

[5] J. Drori, Y. Rosenberg, D. Bermudez, Y. Silberberg and U. Leonhardt, "Observation of Stimulated Hawking Radiation in an Optical Analogue", *Phys. Rev. Lett.* **122** (2019), article no. 010404 (6 pages).

[6] G. Rousseaux, C. Mathis, P. Maïssa, T. G. Philbin and U. Leonhardt, "Observation of negative-frequency waves in a water tank: a classical analogue to the Hawking effect?", *New J. Phys.* **10** (2008), article no. 053015 (12 pages).

[7] S. Weinfurtner, E. W. Tedford, M. C. J. Penrice, W. G. Unruh and G. A. Lawrence, "Measurement of Stimulated Hawking Emission in an Analogue System", *Phys. Rev. Lett.* **106** (2011), article no. 021302 (4 pages).

[8] L.-P. Euvé, F. Michel, R. Parentani, T. G. Philbin and G. Rousseaux, "Observation of noise correlated by the Hawking effect in a water tank", *Phys. Rev. Lett.* **117** (2016), article no. 121301 (5 pages).

[9] J. R. Muñoz de Nova, K. Golubkov, V. I. Kolobov and J. Steinhauer, "Observation of thermal Hawking radiation and its temperature in an analogue black hole", *Nature* **569** (2019), pp. 688–691.

[10] I. Carusotto, S. Fagnocchi, A. Recati, R. Balbinot and A. Fabbri, "Numerical observation of Hawking radiation from acoustic black holes in atomic Bose–Einstein condensates", *New J. Phys.* **10** (2008), article no. 103001 (15 pages).

[11] R. Balbinot, A. Fabbri, S. Fagnocchi, A. Recati and I. Carusotto, "Nonlocal density correlations as a signature of Hawking radiation from acoustic black holes", *Phys. Rev. A* **78** (2008), article no. 021603 (4 pages).

[12] A. Recati, N. Pavloff and I. Carusotto, "Bogoliubov theory of acoustic Hawking radiation in Bose–Einstein condensates", *Phys. Rev. A* **80** (2009), article no. 043603 (10 pages).

[13] J. Macher and R. Parentani, "Black/white hole radiation from dispersive theories", *Phys. Rev. D* **79** (2009), article no. 124008 (23 pages).

[14] P.-É. Larré, A. Recati, I. Carusotto and N. Pavloff, "Quantum fluctuations around black hole horizons in Bose–Einstein condensates", *Phys. Rev. A* **85** (2012), article no. 013621 (16 pages).

[15] X. Busch and R. Parentani, "Quantum entanglement in analogue Hawking radiation: When is the final state nonseparable?", *Phys. Rev. D* **89** (2014), article no. 105024 (14 pages).

[16] S. Finazzi and I. Carusotto, "Entangled phonons in atomic Bose–Einstein condensates", *Phys. Rev. A* **90** (2014), article no. 033607 (9 pages).

[17] J. R. Muñoz de Nova, F. Sols and I. Zapata, "Entanglement and violation of classical inequalities in the Hawking radiation of flowing atom condensates", *New J. Phys.* **17** (2015), article no. 105003 (17 pages).

[18] D. Boiron, A. Fabbri, P.-É. Larré, N. Pavloff, C. I. Westbrook and P. Ziń, "Quantum Signature of Analog Hawking Radiation in Momentum Space", *Phys. Rev. Lett.* **115** (2015), article no. 025301 (5 pages).

[19] A. Finke, P. Jain and S. Weinfurtner, "On the observation of nonclassical excitations in Bose–Einstein condensates", *New J. Phys.* **18** (2016), article no. 113017 (14 pages).

[20] S. Robertson, F. Michel and R. Parentani, "Assessing degrees of entanglement of phonon states in atomic Bose gases through the measurement of commuting observables", *Phys. Rev. D* **96** (2017), article no. 045012 (16 pages).

[21] A. Fabbri and N. Pavloff, "Momentum correlations as signature of sonic Hawking radiation in Bose–Einstein condensates", *SciPost Phys.* **4** (2018), article no. 019 (45 pages).

[22] M. Isoard and N. Pavloff, "Departing from Thermality of Analogue Hawking Radiation in a Bose–Einstein Condensate", *Phys. Rev. Lett.* **124** (2020), article no. 060401 (6 pages). (Accessed on March 26, 2020).

[23] M. Isoard, N. Milazzo, N. Pavloff and O. Giraud, "Bipartite and tripartite entanglement in a Bose–Einstein acoustic black hole", *Phys. Rev. A* **104** (2021), article no. 063302 (28 pages).

[24] G. Ciliberto, S. Emig, N. Pavloff and M. Isoard, "Violation of Bell inequalities in an analog black hole", *Phys. Rev. A* **109** (2024), article no. 063325 (23 pages).

[25] D. D. Solnyshkov, H. Flayac and G. Malpuech, "Black holes and wormholes in spinor polariton condensates", *Phys. Rev. B* **84** (2011), article no. 233405 (4 pages).

[26] D. Gerace and I. Carusotto, "Analog Hawking radiation from an acoustic black hole in a flowing polariton superfluid", *Phys. Rev. B* **86** (2012), article no. 144505 (12 pages).

[27] X. Busch, I. Carusotto and R. Parentani, "Spectrum and entanglement of phonons in quantum fluids of light", *Phys. Rev. A* **89** (2014), article no. 043819 (14 pages).

[28] M. Jacquet, M. Joly, F. Claude, L. Giacomelli, Q. Glorieux, A. Bramati, I. Carusotto and E. Giacobino, "Analogue quantum simulation of the Hawking effect in a polariton superfluid", *Eur. Phys. J. D, Atomic Mol. Opt. Plasma Phys.* **76** (2022), article no. 152 (15 pages).

[29] P. Grišins, H. S. Nguyen, J. Bloch, A. Amo and I. Carusotto, "Theoretical study of stimulated and spontaneous Hawking effects from an acoustic black hole in a hydrodynamically flowing fluid of light", *Phys. Rev. B* **94** (2016), article no. 144518 (12 pages).

[30] S. Robertson, C. Ciret, S. Massar, S.-P. Gorza and R. Parentani, "Four-wave mixing and enhanced analog Hawking effect in a nonlinear optical waveguide", *Phys. Rev. A* **99** (2019), article no. 043825 (21 pages).

[31] A. Choudhary and F. König, "Efficient frequency shifting of dispersive waves at solitons", *Opt. Express* **20** (2012), pp. 5538–5546.

[32] K. Falque, A. Delhom, Q. Glorieux, E. Giacobino, A. Bramati and M. J. Jacquet, "Polariton Fluids as Quantum Field Theory Simulators on Tailored Curved Spacetimes", *Phys. Rev. Lett.* **135** (2025), article no. 023401 (7 pages).

[33] M. J. Jacquet, L. Giacomelli, Q. Valnais, et al., "Quantum Vacuum Excitation of a Quasinormal Mode in an Analog Model of Black Hole Spacetime", *Phys. Rev. Lett.* **130** (2023), article no. 111501 (6 pages).

[34] M. Jacquet and F. König, "The influence of spacetime curvature on quantum emission in optical analogues to gravity", *SciPost Phys. Core* **3** (2020), article no. 005 (15 pages). (Accessed on September 30, 2020).

[35] I. Carusotto and C. Ciuti, "Quantum fluids of light", *Rev. Mod. Phys.* **85** (2013), pp. 299–366.

[36] K. Guerrero, K. Falque, E. Giacobino, A. Bramati and M. J. Jacquet, "Multiply quantized vortex spectroscopy in a quantum fluid of light", preprint, 2025. Online at https://arxiv.org/abs/2507.14539.

[37] M. Visser, "Acoustic black holes: horizons, ergospheres and Hawking radiation", *Class. Quant. Grav.* **15** (1998), no. 6, article no. 1767.

[38] Y. Castin, "Bose–Einstein Condensates in Atomic Gases: Simple Theoretical Results", in *Coherent atomic matter waves* (R. Kaiser, C. Westbrook and F. David, eds.), Les Houches - École d'Été de Physique Theorique, Springer, 2001, pp. 1–136.

[39] A. Delhom, K. Guerrero, P. Calizaya Cabrera, K. Falque, A. Bramati, A. J. Brady, M. J. Jacquet and I. Agullo, "Entanglement from superradiance and rotating quantum fluids of light", *Phys. Rev. D* **109** (2024), article no. 105024 (24 pages).

[40] E. Berti, V. Cardoso and J. P. S. Lemos, "Quasinormal modes and classical wave propagation in analogue black holes", *Phys. Rev. D* **70** (2004), article no. 124006 (17 pages).

[41] P. Lalanne, W. Yan, K. Vynck, C. Sauvan and J.-P. Hugonin, "Light Interaction with Photonic and Plasmonic Resonances", *Laser Photonics Rev.* **12** (2018), article no. 1700113 (38 pages).

[42] F. D. Porro, S. Liberati and M. Schneider, "Tunneling method for Hawking quanta in analogue gravity", *Comptes Rendus. Physique* **25** (2024), pp. 1–27.

[43] R. Parentani, "From vacuum fluctuations across an event horizon to long distance correlations", *Phys. Rev. D* **82** (2010), article no. 025008 (17 pages).

[44] C. Barcelo, S. Liberati, S. Sonego and M. Visser, "Hawking-like radiation from evolving black holes and compact horizonless objects", *J. High Energy Phys.* **2011** (2011), article no. 3 (29 pages).

[45] S. Finazzi and R. Parentani, "On the robustness of acoustic black hole spectra", *J. Phys. Conf. Ser.* **314** (2011), article no. 012030 (4 pages).

[46] S. Finazzi and R. Parentani, "Spectral properties of acoustic black hole radiation: Broadening the horizon", *Phys. Rev. D* **83** (2011), article no. 084010 (13 pages).

[47] A. Fabbri and R. Balbinot, "Ramp-up of Hawking Radiation in Bose–Einstein-Condensate Analog Black Holes", *Phys. Rev. Lett.* **126** (2021), article no. 111301 (6 pages).

[48] I. Agullo, A. J. Brady, A. Delhom and D. Kranas, "Entanglement from rotating black holes in thermal baths", *Phys. Rev. D* **110** (2024), article no. 025021 (16 pages).

[49] J. W. York, "Dynamical origin of black-hole radiance", *Phys. Rev. D* **28** (1983), pp. 2929–2945.

[50] S. Hod, "Bohr's Correspondence Principle and the Area Spectrum of Quantum Black Holes", *Phys. Rev. Lett.* **81** (1998), pp. 4293–4296.

[51] M. Maggiore, "Physical Interpretation of the Spectrum of Black Hole Quasinormal Modes", *Phys. Rev. Lett.* **100** (2008), article no. 141301 (4 pages).